



CHORUS

This is the accepted manuscript made available via CHORUS. The article has been published as:

First-principles study of band gap engineering via oxygen vacancy doping in perovskite ABO_3 solid solutions

Tingting Qi, Matthew T. Curnan, Seungchul Kim, Joseph W. Bennett, Ilya Grinberg, and Andrew M. Rappe

Phys. Rev. B **84**, 245206 — Published 15 December 2011

DOI: [10.1103/PhysRevB.84.245206](https://doi.org/10.1103/PhysRevB.84.245206)

A First-principles Study of Band Gap Engineering via Oxygen Vacancy Doping in $ABB'O_3$ Perovskite Solid Solutions

Tingting Qi, Matthew T. Curnan, Seungchul Kim, Joseph W. Bennett, Ilya Grinberg and Andrew M. Rappe*

*The Makineni Theoretical Laboratories, Department of Chemistry
University of Pennsylvania, Philadelphia, PA 19104-6323*

(Dated: October 31, 2011)

Oxygen vacancies in perovskite oxide solid solutions are fundamentally interesting and technologically important. However, experimental characterization of the vacancy locations and their impact on electronic structure is challenging. We have carried out first-principles calculations on two Zr-modified solid solutions, $\text{Pb}(\text{Zn}_{1/3}\text{Nb}_{2/3})\text{O}_3$ and $\text{Pb}(\text{Mg}_{1/3}\text{Nb}_{2/3})\text{O}_3$, in which vacancies are present. We find that the vacancies are more likely to reside between low-valent cation-cation pairs than high-valent cation-cation pairs. Based on the analysis of our results, we formulate guidelines that can be used to predict the location of oxygen vacancies in perovskite solid solutions. Our results show that vacancies can have a significant impact on both the conduction and valence band energies, in some cases lowering the band gap by ≈ 0.5 eV. The effects of vacancies on the electronic band structure can be understood within the framework of crystal field theory.

PACS numbers: 77.84.Lf, 71.15.-m, 71.20.-b

I. INTRODUCTION

Ferroelectric perovskite (ABO_3) oxides are used in a wide range of applications that include transducers, SONAR, and non-volatile random access memory (NVRAM)^{1,2}. Oxygen vacancy defects are frequently found in these ABO_3 oxides and can significantly affect their properties. For example, fatigue in the switching of ferroelectric NVRAM devices has been ascribed to oxygen vacancies pinning domain walls³. A high concentration of oxygen vacancies is also associated with degraded dielectric and piezoelectric properties^{4,5}. In other cases, oxygen vacancies can play a beneficial role. For example, in solid oxide fuel cells, oxygen vacancies enable transport of O^{2-} ions through the oxide electrolyte membrane over a range of temperatures. In solar energy research, recent theoretical work has shown that ferroelectric perovskites modified by M^{2+} -O vacancy substitution ($M = \text{Ni}, \text{Pd}, \text{Pt}$) exhibit a low band gap and a high polarization, making them suitable for photovoltaic applications⁶⁻⁸.

Despite the technological relevance of oxygen vacancies in ferroelectric perovskite solid solutions, the energetics of vacancy location preference in these materials has not been thoroughly studied. Although there have been a few recent spectroscopic breakthroughs in locating oxygen vacancies⁹, the atomic-scale resolution of oxygen vacancy positions is still difficult to achieve experimentally. This makes density functional theory (DFT) calculations a natural approach for studying vacancies, due to the combination of atomic scale resolution, computational efficiency, and accuracy.

Recent experimental work showed that a high oxygen-vacancy content could be achieved by substituting Zr^{4+} for Nb^{5+} ions in the ferroelectric relaxor material $\text{Pb}(\text{Mg}_{1/3}\text{Nb}_{2/3})\text{O}_3$ (PMN). This substitution was also shown to promote B -cation ordering in the resultant $\text{Pb}(\text{Mg}_{1/3}\text{Zr}_{2x/3}\text{Nb}_{2(1-x)/3})\text{O}_{3-x/3}$ solid solution for $x < 0.2$ ^{10,11}. Concurrently, our recent theoretical study has

demonstrated that changes to the coordination environment of Zn^{2+} in ferroelectrics can lead to a large reduction in the band gap¹². In this work, we use DFT calculations to study the Zr-modified solid solutions $\text{Pb}(\text{Zn}_{1/3}\text{Nb}_{2/3})\text{O}_3$ (Zr-PZN) and $\text{Pb}(\text{Mg}_{1/3}\text{Nb}_{2/3})\text{O}_3$ (Zr-PMN) and investigate vacancy energetics and the impact of vacancies on the band structure.

II. METHODOLOGY

We studied several chemical compositions and different cation arrangements for the two Zr-modified solid solutions, Zr-PZN and Zr-PMN. For each cation arrangement, vacancy locations between different B -cation pairs were examined. We used the Quantum ESPRESSO package¹³ to relax the internal ionic coordinates and lattice parameters of the solid solutions. Initial lattice constants were chosen based on Shannon-Prewitt ionic radii¹⁴, and all atoms are represented by norm-conserving optimized¹⁵ nonlocal¹⁶ pseudopotentials generated using the OPIUM code¹⁷. All calculations were performed with a plane-wave basis set¹⁸ with an energy cutoff of 55 Ry. The local density approximation (LDA-PZ)¹⁹ and a $6 \times 6 \times 6$ Monkhorst-Pack k -point sampling of the Brillouin zone²⁰ relative to a 5-atom unit cell were applied. The orbital-projected densities of states (PDOS)^{21,22} were calculated with $12 \times 12 \times 12$ k -point meshes relative to a 5-atom unit cell. The generalized gradient approximation (GGA-PBE)²³ exchange-correlation functional was also used for some structures to confirm that the GGA results are qualitatively consistent with those obtained by LDA calculations.

In pure PMN, the B -cation arrangement follows 1:1 long-range order; along the $\{111\}$ directions, the $\{111\}$ planes of B -cations alternate between full occupancy by Nb^{5+} (B'' sublattice) and random occupancy by Mg^{2+} and the remaining Nb^{5+} (B' sublattice). In Zr-PMN, it

was experimentally determined by x-ray diffraction scanning electron microscopy and that the dopant Zr^{4+} ions replace Nb^{5+} only on the B' sublattice¹⁰. This leads to enhanced charge and size differences between B' and B'' cations with increasing Zr substitution.¹⁰ Due to the compositional similarity between PMN- and PZN-derived solid solutions and the fact that they often exhibit a 1:1 B -site order in accordance with the random site model²⁴, we expect the dopant Zr^{4+} to only replace Nb^{5+} on the B' sublattice in Zr-modified PZN as well.

When Nb^{5+} is replaced by Zr^{4+} , oxygen vacancies are generated to maintain charge neutrality. If 1:1 B -site order is enforced, there are only three possible nearest-neighbor B -cation pairs for any oxygen vacancy: M -vac-Nb, Nb-vac-Nb, and Zr-vac-Nb for $M = \text{Mg}$ or Zn . To study a composition with low Zr content, 1:1 B -site order, relatively large vacancy-vacancy separation and all three possible types of vacancy locations, we use a 119-atom supercell, with a chemical composition $\text{Pb}(M_{0.333}\text{Nb}_{0.583}\text{Zr}_{0.083})\text{O}_{2.958}$, labeled “C” in Fig. 1. In addition, two other chemical compositions without 1:1 B -cation order were investigated using 39-atom supercells, labeled “A” ($\text{Pb}(M_{0.25}\text{Nb}_{0.25}\text{Zr}_{0.5})\text{O}_{2.875}$) and “B” ($\text{Pb}(M_{0.375}\text{Nb}_{0.5}\text{Zr}_{0.125})\text{O}_{2.875}$). Four different cation arrangements were analyzed for each of the two compositions “A” and “B”.

Due to computational cost constraints, we investigated only a subset of the the many possible B -cation configurations for the present study. We chose supercells that contain chemically different B -cation arrangements. The similarities in the DFT-obtained energy differences show that the overall B -cation arrangement of the supercell has only a secondary impact on the vacancy position energetics (Table I). This suggests that our sampling of the possible B -cation configurations is representative of the behavior found in the real material where all possible configurations are present.

It is important to note that in Table I, some vacancy locations are not present for certain cation arrangements. In some cases, it is due to the presence of 1:1 B -site order, which forbids cation arrangements such as M -vac- M . In other cases, the oxygen vacancy migrates away from its initial position during the ionic relaxation, indicating that some sites are highly unfavorable vacancy locations. For example, in the case of the Zr-modified PZN cation arrangement A3, the oxygen vacancy moves from an initial position between two Nb^{5+} to a final position between Nb^{5+} and Zn^{2+} .

III. RESULTS

A. Vacancy Energetics

The results for Zr-modified PZN presented in Table I show that regardless of cation arrangement, oxygen vacancies always prefer to reside between two Zn^{2+} . The observed trend in vacancy position ener-

getics is $E_{\text{Zr-vac-Zr}} > E_{\text{Nb-vac-Zr}} > E_{\text{Nb-vac-Nb}} > E_{\text{Zr-vac-Zn}} > E_{\text{Nb-vac-Zn}} > E_{\text{Zn-vac-Zn}}$. For structures with 1:1 B -cation order, such as C1 and C2, Nb-vac-Zn is the most favored. We find that the vacancy location preference is closely related to the reference displacement magnitude, D_M^0 , of the two cations adjacent to the vacancy. D_M^0 is defined as the displacement that a cation will make when placed in an almost pure PbTiO_3 solid solution, and was previously found to play a key role in determining the overall structure of the ferroelectric perovskite solid solutions²⁵. More covalent ions (such as Zn , $D_{\text{Zn}}^0 = 0.25 \text{ \AA}$) usually exhibit larger D_M^0 than more ionic ions (such as Mg , $D_{\text{Mg}}^0 = 0.08 \text{ \AA}$)²⁵⁻²⁷.

We find that in Zr-modified PZN, oxygen vacancies tend to reside between two B -cations that have the largest average D_M^0 . The ranking of the average D_M^0 of the two nearest neighbor B -cations of the vacancy is $D_{\text{Zr-vac-Zr}}^0 < D_{\text{Nb-vac-Zr}}^0 < D_{\text{Nb-vac-Nb}}^0 < D_{\text{Zr-vac-Zn}}^0 < D_{\text{Nb-vac-Zn}}^0 < D_{\text{Zn-vac-Zn}}^0$. This ranking is the exact inverse of the trend in the vacancy position energy differences for all of the compositions. (Figure 2)

Based on the results for Zr-modified PZN, we should expect Nb-vac-Nb to be the most preferred structure in Zr-modified PMN, since Nb^{5+} shows the largest D_M^0 . However, our calculations for Zr-modified PMN show that the Mg-vac-Mg configuration is the most energetically favored, despite the fact that D_{Mg}^0 (0.08 \AA) is the smallest reference displacement among all the cations. This indicates that D_M^0 is not the sole determining factor for vacancy position energetics. The obvious difference between Mg^{2+} and other cations is its small valence. Therefore, we infer that the low valence of Mg^{2+} is responsible for the low energy of the Mg-vac-Mg arrangement, as the vacancy disrupts the smallest number of chemical bonds, leading to a lower energy cost. The results of both Zr-modified PZN and PMN calculations demonstrate that an oxygen vacancy prefers a location between two B -cations that have *both* low valence and large D_M^0 .

Our finding that Mg-vac-Mg and Nb-vac-Mg structures are the most energetically favored contradicts the previous experimental conclusions of Zhao *et al.*¹⁰. In that study, the authors investigated bulk ceramics using X-ray diffraction and SEM techniques, which suggest that based on the dependence of the B -cation ordering on Zr fraction, Nb-vac-Nb structures have the lowest energy in Zr-modified PMN solid solution $\text{Pb}(\text{Mg}_{1/3}\text{Zr}_{2x/3}\text{Nb}_{2(1-x)/3})\text{O}_{3-x/3}$. Zhao *et al.* assumed that Nb-vac-Nb is the most preferred configuration due to Nb^{5+} stability in five-fold coordinated environment. When x is smaller than 0.20, it is possible for an oxygen vacancy to find one Nb^{5+} on the B' sublattice and another Nb^{5+} on the B'' sublattice, since Nb^{5+} on B' sublattice is more abundant than the introduced vacancies. When x reaches a value higher than 0.20, then Nb-vac-Nb arrangement cannot be satisfied for most of the oxygen vacancies, which breaks the long-range cation order. However, until that composition is reached, higher

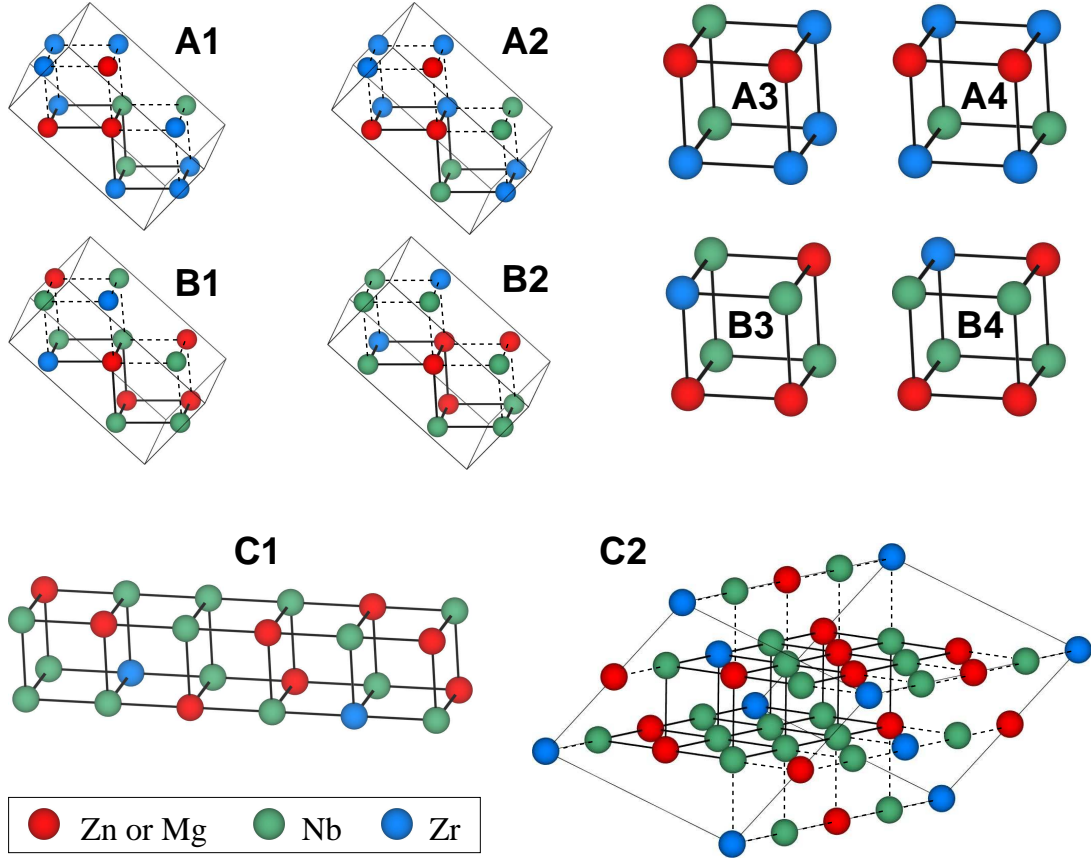


FIG. 1: (Color online) Supercells used in this study. A-cations and O atoms are omitted for clarity. The supercell dimensions for A1, A2, B1, and B2 are $\sqrt{2} \times 2 \times 2\sqrt{2}$, and $2 \times 2 \times 2$ for A3, A4, B3, and B4. C1 and C2 supercells are $6 \times 2 \times 2$ and $\sqrt{6} \times 2\sqrt{2} \times 4$, respectively.

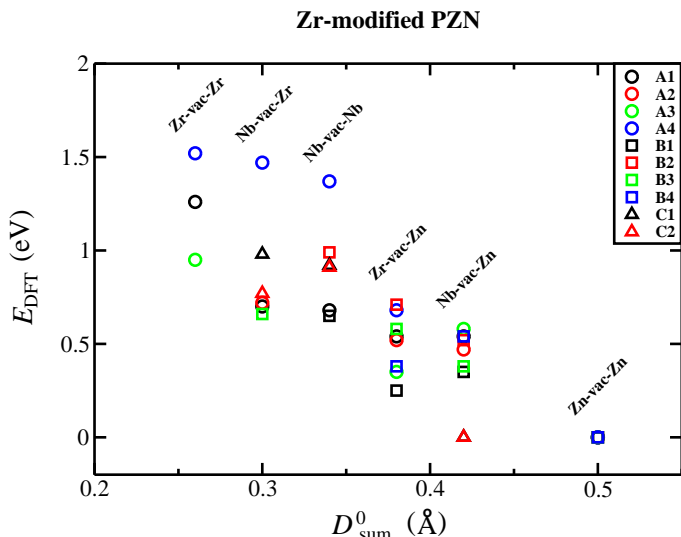


FIG. 2: (Color online) Energy per supercell versus the displacement tendency D_{sum}^0 of the B -cation neighbors in Zr-modified PZN. Shown are the energy differences between the total energy of each structure and that of the lowest-energy structure with the same cation ordering (as in Table I). A clear inverse trend is apparent, with a larger D_{sum}^0 corresponding to a lower DFT-calculated energy difference.

Zr content favors long-range B -cation order due to the increased size and charge difference between the B' and the B'' sublattices (with greater Zr fraction). These two trends predict that the peak B -cation order should be reached at $x=0.20$. Experimentally, Zhao *et al.* found a peak in B -cation ordering at $x=0.15$, in reasonable agreement with the expected peak B -cation order x based on the arguments above. They therefore concluded that Nb-vac-Nb is the most preferred vacancy configuration in Zr-modified PMN.

However, our calculations found that when 1:1 B -cation order is enforced in Zr-modified PMN, Nb-vac-Mg structures are the lowest in energy. This implies a greater flexibility for all vacancies to find their preferred B -cation neighbors, with one Nb on B'' sublattice and one Mg on the B' sublattice in a 1:1 B -cation ordered material. Even at higher vacancy concentrations, there are sufficient Mg^{2+} (two thirds of B' sublattice sites) to have Nb-vac-Mg configurations. Therefore, the decline in the B -cation ordering cannot be attributed to the lack of the Nb-vac-Nb configurations. Rather, it is likely that vacancy-vacancy repulsive interactions play a key role. These interactions can be quite strong when the two vacancies are in close proximity. For example, in CaTiO_3 , there is a 0.5-1.5 eV energy cost for a vacancy-vacancy separation of 4 Å²⁸. Therefore, as x increases, the configurations with two vacancies close to each other must be considered.

When the vacancy concentration is low, the preference to avoid short vacancy-vacancy distances and the preference for the Nb-vac-Mg configuration can be satisfied

simultaneously. As a result, the increased charge and size differences between the two B -cation sublattices enhance B -cation ordering. However, when the vacancy concentration is high, the vacancy-vacancy interactions become dominant. It becomes increasingly difficult to simultaneously separate the vacancies and fulfill the Nb-vac-Mg preference in the framework of a 1:1 long-range B -cation ordering. Our results show that without the 1:1 B -cation ordering, Nb-vac-Mg and Nb-vac-Zr configurations have about the same energy and Mg-vac-Mg becomes the most preferable. This greater flexibility makes it easier to avoid large energy costs of vacancy-vacancy repulsion. As a result, at higher vacancy concentration, the long-range B -cation order is destabilized. Since the destabilization depends on two vacancies being in close proximity to one another, it scales as x^2 and becomes important only at higher x , leading to a nonmonotonic dependence of the B -cation order on Zr^{4+} composition.

B. Electronic Band Gap

We now describe how oxygen vacancies modify the electronic structure in Zr-doped PZN and PMN. For both pure PZN and pure PMN with 1:1 B -cation order (30-atom supercell), our calculated LDA band gap is around 2.2 eV. For the antiferroelectric PbZrO_3 (PZ, $Pbam$ symmetry, 40-atom supercell)²⁹, our LDA band gap is about 2.5 eV. We therefore expect a mixture of PZN-PZ or PMN-PZ *without* oxygen vacancies to exhibit band gap values in the 2.2-2.5 eV range.

For Zr-modified PZN, the band gaps vary depending on the vacancy location and the cation arrangement and can be as low as 1.7 eV. Interestingly, we found that when the cation arrangement contains an alternating $\cdots\text{Zn-O-Zn-O}\cdots$ chain (A3, A4, B2, B3, and B4), the corresponding band gap values are systematically 0.2-0.3 eV lower than those of the remaining arrangements, namely A1, A2, B1, C1, and C2. To understand this effect, we compare projected densities of states (PDOS) for five different structures: Zn-vac-Zn for the A1, A3 and A4 supercells, Zn-vac-Nb for the A3 supercell, and Zr-vac-Zn for the A4 supercell (Fig. 3). We investigate the atomic orbital compositions of both the valence band maximum (VBM) and the conduction band minimum (CBM).

First, we compare the results for the Zn-vac-Zn A1 and A4 supercells (Figure 3). There is an alternating $\cdots\text{Zn-O-Zn-O}\cdots$ chain present in A4, but not in A1. In the A1 supercell, we found that the CBM consists of Pb $6p$ and the VBM contains mainly the O $2p$ orbitals. On the other hand, in the A4 supercell, while the CBM also chiefly consists of Pb $6p$, the VBM comes from Zn $3d_{z^2}$, Zn $3d_{x^2-y^2}$, and O $2p$ orbitals of the oxygen atoms in the vicinity of the vacancy.

The rise of the Zn $3d_{z^2}$ and $3d_{x^2-y^2}$ orbitals to the top of the valence band can be explained by crystal field theory. The removal of an oxygen atom to create a vacancy reduces the coordination number of the two neighboring

TABLE I: A comparison of Zr-modified PZN and PMN structures with different chemical compositions (A, B, and C) and different cation arrangements. E_{DFT} represents the relative energy of each structure relative to the lowest energy structure within the same cation ordering, while E_g specifies the band gaps (both in eV). V_{sum} , R_{sum} , and D_{sum}^0 are the summations of the charge valence, ionic radii (\AA), and displacement tendency (\AA) of the oxygen vacancy's two closest B -cation neighbors, respectively.

Cation ordering	PZN-PZ						PMN-PZ					
	vac. position	E_{DFT}	V_{sum}	R_{sum}	D_{sum}^0	E_g	vac. position	E_{DFT}	V_{sum}	R_{sum}	D_{sum}^0	E_g
A1	Zr-vac-Zr	1.26	8	1.44	0.26	2.29	Zr-vac-Zr	0.76	8	1.44	0.26	2.21
	Nb-vac-Zr	0.70	9	1.36	0.30	2.19	Nb-vac-Mg	0.39	7	1.36	0.25	2.11
	Nb-vac-Nb	0.68	10	1.28	0.34	2.28	Nb-vac-Nb	0.36	10	1.28	0.34	2.21
	Zr-vac-Zn	0.54	6	1.46	0.38	2.31	Zr-vac-Mg	0.33	6	1.44	0.21	2.27
	Nb-vac-Zn	0.54	7	1.38	0.42	2.04	Nb-vac-Zr	0.30	9	1.36	0.30	2.22
	Zn-vac-Zn	0.00	4	1.48	0.50	2.44	Mg-vac-Mg	0.00	4	1.44	0.16	2.40
A2	Nb-vac-Zr	0.72	9	1.36	0.30	2.30	Nb-vac-Nb	1.08	10	1.28	0.34	1.92
	Zr-vac-Zn	0.52	6	1.46	0.38	2.15	Zr-vac-Zr	0.86	8	1.44	0.26	1.96
	Nb-vac-Zn	0.47	7	1.38	0.42	2.25	Nb-vac-Mg	0.47	7	1.36	0.25	2.17
	Zn-vac-Zn	0.00	4	1.48	0.50	2.40	Nb-vac-Zr	0.38	9	1.36	0.30	2.28
A3	Zr-vac-Zr	0.95	8	1.44	0.26	2.12	Mg-vac-Mg	0.00	4	1.44	0.16	2.36
	Nb-vac-Zn	0.58	7	1.38	0.42	2.01	Zr-vac-Zr	1.00	8	1.44	0.26	2.04
	Zr-vac-Zn	0.35	6	1.46	0.38	2.04	Nb-vac-Zr	0.98	9	1.36	0.30	1.97
	Zn-vac-Zn	0.00	4	1.48	0.50	2.17	Nb-vac-Nb	0.92	10	1.28	0.34	2.00
							Mg-vac-Zr	0.52	6	1.44	0.21	2.07
A4	Zr-vac-Zr	1.52	8	1.44	0.26	1.88	Mg-vac-Mg	0.00	4	1.44	0.16	2.18
	Nb-vac-Zr	1.47	9	1.36	0.30	1.79	Zr-vac-Zr	0.60	8	1.44	0.26	2.12
	Nb-vac-Nb	1.37	10	1.28	0.34	1.92	Nb-vac-Mg	0.41	7	1.36	0.25	2.01
	Zr-vac-Zn	0.68	6	1.46	0.38	1.73	Zr-vac-Mg	0.36	6	1.44	0.21	2.02
	Zn-vac-Zn	0.00	4	1.48	0.50	2.12	Mg-vac-Mg	0.00	4	1.44	0.16	2.12
B1	Nb-vac-Nb	0.65	10	1.28	0.34	2.41	Nb-vac-Nb	0.13	10	1.28	0.34	2.28
	Nb-vac-Zn	0.35	7	1.38	0.42	2.11	Nb-vac-Mg	0.12	7	1.38	0.25	2.20
	Zr-vac-Zn	0.25	6	1.46	0.38	2.41	Zr-vac-Mg	0.06	6	1.44	0.21	2.35
	Zn-vac-Zn	0.00	4	1.48	0.50	2.36	Mg-vac-Mg	0.00	4	1.44	0.16	2.28
B2	Nb-vac-Nb	0.99	10	1.28	0.34	2.22	Zr-vac-Mg	0.38	6	1.44	0.21	2.18
	Zr-vac-Zn	0.71	6	1.46	0.38	2.05	Nb-vac-Nb	0.17	10	1.28	0.34	2.10
	Nb-vac-Zn	0.52	7	1.38	0.42	2.11	Nb-vac-Mg	0.13	7	1.36	0.25	2.16
	Zn-vac-Zn	0.00	4	1.48	0.50	2.10	Mg-vac-Mg	0.00	4	1.44	0.16	2.21
B3	Nb-vac-Zr	0.66	9	1.36	0.30	2.10	Zr-vac-Mg	0.59	6	1.44	0.21	2.13
	Zr-vac-Zn	0.58	6	1.46	0.38	2.17	Nb-vac-Mg	0.48	7	1.36	0.25	2.02
	Nb-vac-Zn	0.38	7	1.38	0.42	2.06	Mg-vac-Mg	0.00	4	1.44	0.16	2.32
	Zn-vac-Zn	0.00	4	1.48	0.50	2.11						
B4	Nb-vac-Zn	0.54	7	1.38	0.42	2.08	Nb-vac-Mg	0.47	7	1.36	0.25	2.10
	Zr-vac-Zn	0.38	6	1.46	0.38	2.14	Zr-vac-Mg	0.23	6	1.44	0.21	2.15
	Zn-vac-Zn	0.00	4	1.48	0.50	2.28	Mg-vac-Mg	0.00	4	1.44	0.16	2.24
C1	Nb-vac-Zr	0.98	9	1.36	0.30	2.10	Nb-vac-Zr	0.66	9	1.36	0.30	2.24
	Nb-vac-Nb	0.92	10	1.28	0.34	2.13	Nb-vac-Nb	0.62	10	1.28	0.34	2.16
	Nb-vac-Zn	0.00	7	1.38	0.42	2.22	Nb-vac-Mg	0.00	7	1.36	0.25	2.26
C2	Nb-vac-Nb	0.91	10	1.28	0.34	2.21	Nb-vac-Nb	0.56	10	1.28	0.34	2.32
	Nb-vac-Zr	0.77	9	1.36	0.30	2.30	Nb-vac-Zr	0.40	9	1.36	0.30	2.33
	Nb-vac-Zn	0.00	7	1.38	0.42	2.30	Nb-vac-Mg	0.00	7	1.36	0.25	2.34

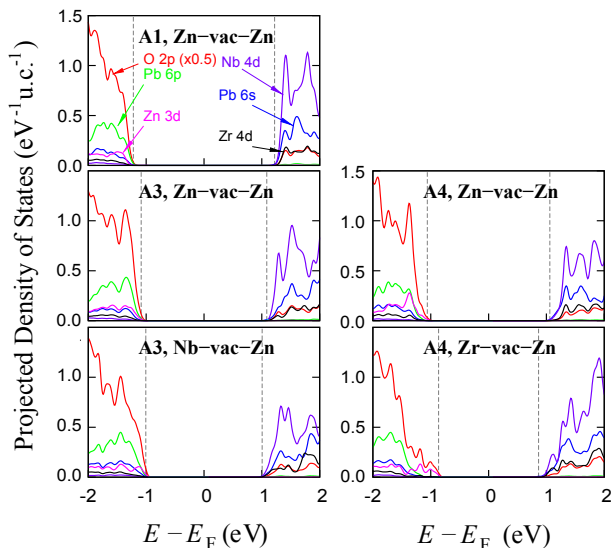


FIG. 3: (Color online) Projected density of states results for Zn-vac-Zn structure for supercell A1 ($E_g = 2.44$ eV), Zn-vac-Zn structure for supercell A3 ($E_g = 2.17$ eV), Nb-vac-Zn structure for supercell A3 ($E_g = 2.01$ eV), Zn-vac-Zn structure for supercell A4 ($E_g = 2.12$ eV) and Zr-vac-Zn structure for supercell A4 ($E_g = 1.73$ eV). The oxygen PDOS are divided by 2 for ease of comparison. In the y axis label, u.c. stands for a 5-atom unit cell of perovskite. The two dashed lines in each panel indicate the energy levels of VBM and CBM.

Zn²⁺ ions from six to five, altering the Zn-O bonding geometry from an octahedral arrangement to a square pyramid. According to crystal field theory, this changes the energy splitting of the 3d orbitals by lifting the degeneracy of the Zn $3d_{x^2-y^2}$ and $3d_{z^2}$ orbitals relative to the octahedral arrangement ($3d_{x^2-y^2}$ becomes higher in energy than $3d_{z^2}$) and pushing them toward the top of the valence band. For cation arrangements with alternating \cdots -Zn-O-Zn-O- \cdots chains, the oxygen atoms between the two Zn²⁺ are underbonded. Therefore, these O atoms make stronger bonds with their neighboring Pb atoms. The stronger Pb-O bonds with higher charge density increase the repulsive interaction between Zn 3d and the charge in the Pb-O bonds, further raising the energies of Zn $3d_{z^2}$ and Zn $3d_{x^2-y^2}$ orbitals and lifting them to the valence band maximum. This is apparent in the PDOS for the Zn-vac-Zn structure in supercell A4). Such an increased energy of the VBM leads to a 0.3 eV smaller band gap of Zn-vac-Zn structure for supercell A4 compared to the band gap of the Zn-vac-Zn structure for supercell A1. A similar crystal chemical effect on the energies of the Zn d states and the band gap was found for the extremely tetragonal Bi(Zn_{1/2}Ti_{1/2})O₃ material.¹²

The repulsive interaction between the charge density in the Pb-O bonds and the Zn d_{z^2} and Zn $3d_{x^2-y^2}$ orbitals also causes the upshift of the VBM for the Zr-vac-Zn A4 structure compared to the Zn-vac-Zn A4 structure. When the vacancy is located between the two Zn

atoms, each Zn has only one underbonded O atom neighbor along the \cdots -Zn-O-Zn-O- \cdots chain. However, when the vacancy is located between Zn and Zr or Zn and Nb, each Zn has two underbonded O atom neighbors along the \cdots -Zn-O-Zn-O- \cdots chain. This means that twice as many strong Pb-O bonds are present in the vicinity of Zn $3d_{z^2}$ and Zn $3d_{x^2-y^2}$ orbitals for the Zr-vac-Zn compared to Zn-vac-Zn. This gives rise to stronger repulsive interactions and a greater upshift in the Zn d_{z^2} and $3d_{x^2-y^2}$ energy levels, raising the VBM of Zr-vac-Zn compared to Zn-vac-Zn.

Coordination changes and the effect of the Pb-O charge density repulsion also impact the energies of the unfilled Nb 4d orbitals in the conduction band. For example, Figure 3 shows that in both Zn-vac-Zn and Zn-vac-Nb vacancy sites in the A3 cation arrangement, the VBM is composed of Zn $3d_{z^2}$, Zn $3d_{x^2-y^2}$, and O 2p orbitals; however, the conduction band minima of the two systems are different. For Zn-vac-Nb in the A3 supercell, the CBM contains Nb $4d_{xz}$, Nb $4d_{yz}$, and Pb 6p, while for Zn-vac-Zn in the A3 supercell, only Pb 6p orbitals are found at the CBM. This difference can also be explained by crystal field theory. The decrease in the Nb-O coordination number increases the energy splitting for Nb 4d orbitals, pushing the energy of Nb $4d_{xz}$ and Nb $4d_{yz}$ orbital to the bottom of the conduction band and lowering the energy of CBM. Thus, for Zn-vac-Nb structure in the A3 supercell, the combined effects of a higher-energy VBM and a lower-energy CBM resulting from the presence of the vacancy lead to the lowest supercell A3 band gap.

Comparison of the Zn-vac-Zn and Zr-vac-Zn structures of supercell A4 (Figure 3) illustrates the impact of the changes in the repulsion from the Pb-O bond charge density on the energy levels of the unfilled Nb 4d states. When the vacancy is located between two Zn atoms, the Pb atom off-centers away from the vacancy and toward the underbonded O atoms located between Zr and Zn. On the other hand, when the vacancy is located between Zr and Zn, Pb atom off-center displacement will be directed toward the severely underbonded O atom between two Zn. In this case, the strong Pb-O bond will be pointing directly away from the two Nb atoms, lessening the repulsive interactions between the charge density in Pb-O bonds and the Nb 4d orbitals. A weaker repulsion interaction lowers the energy of the Nb 4d states for the Zr-vac-Zn states and contributes to the decrease of the band gap for Zr-vac-Zn structure relative to the Zn-vac-Zn structure.

For Zr-modified PMN, the band gap values range from 1.9 eV to 2.4 eV, depending on the vacancy location and cation arrangement, with either Nb-vac-Mg or Nb-vac-Nb exhibiting the lowest E_g . The decrease in the band gap can be explained by crystal field theory arguments presented above. Even though the Mg²⁺-O bonding interaction changes due to the vacancy in these cases, these changes do not affect the VBM. This is because the Mg 2p orbitals are located far below the VBM. The band gap decrease comes solely from lowering of the CBM, caused

by the change in the B -cation coordination and repulsive interactions with the charge density of Pb-O bonds and the resulting enhancement in the energy splitting of the Nb $4d$ orbitals. This makes the range of band gap values smaller in Zr-modified PMN than in the Zr-modified PZN.

IV. CONCLUSIONS

In conclusion, oxygen vacancies were found to prefer locations between two B -cations with a lower combined valence and a larger covalency. Cations that meet these criteria show the largest capacity for accommodating a vacancy. Previous work has shown that a decrease in the band gap can be achieved by variation in the B -cation arrangement in ferroelectric materials with extremely large tetragonality; in this paper, the same crystal field theory principle is used in a different band gap engineering strategy. Here, extreme structural features are unnecessary, rather a change in the cation coordination due to the presence of a vacancy is sufficient. In order to obtain a

lower band gap, proper B -cation species must be selected, ensuring that their atomic orbital contributions are in the vicinity of the CBM and VBM. When such low-valence cations are aligned in chains, vacancy-induced changes in the electronic structure can lower the band gap by up to 0.5 eV.

V. ACKNOWLEDGMENTS

T. Q., S. C. K., and I. G. were supported by the Office of Naval Research, under grant numbers N00014-09-1-0157, N00014-11-1-0664 and N00014-11-1-0578. J. W. B. was supported by the Department of Energy Office of Basic Energy Sciences, under grant number DE-FG02-07ER46431. M. T. C. and A. M. R. were supported by Air Force Office of Scientific Research, under grant FA9550-10-1-0248. Computational support was provided by US DoD, by a DURIP grant and by a Challenge Grant from the HPCMO. We would like to acknowledge D. Vincent West and Peter K. Davies for many helpful discussions.

-
- * corresponding author: rappe@sas.upenn.edu
- ¹ S.-E. Park and T. R. Shrout, *J. Appl. Phys.* **82**, 1804 (1997).
 - ² J. F. Scott, *Science* **315**, 954 (2007).
 - ³ H. M. Duiker, P. D. Beale, J. F. Scott, C. A. P. Dearaujo, B. M. Melnick, J. D. Cuchiaro, and L. D. McMillan, *J. Appl. Phys.* **68**, 5783 (1990).
 - ⁴ J. F. Scott and M. Dawber, *Appl. Phys. Lett.* **76**, 3801 (2000).
 - ⁵ M. Dawber and J. F. Scott, *Appl. Phys. Lett.* **76**, 1060 (2000).
 - ⁶ J. W. Bennett, I. Grinberg, and A. M. Rappe, *J. Am. Chem. Soc.* **130**, 17409 (2008).
 - ⁷ J. W. Bennett, I. Grinberg, P. K. Davies, and A. M. Rappe, *Phys. Rev. B* **82**, 184106 (2010).
 - ⁸ G. Y. Gou, J. W. Bennett, H. Takenaka, and A. M. Rappe, *Phys. Rev. B* **83**, 205115 (2011).
 - ⁹ R. A. Eichel, *Phys. Chem. Chem. Phys.* **13**, 368 (2011).
 - ¹⁰ X. Zhao, W. Qu, and X. Tan, *J. Am. Ceram. Soc.* **91**, 3031 (2008).
 - ¹¹ X. Zhao, W. Qu, X. Tan, A. A. Bokov, and Z.-G. Ye, *Phys. Rev. B* **79**, 114101 (2009).
 - ¹² T. Qi, I. Grinberg, and A. M. Rappe, *Phys. Rev. B* **83**, 224108 (2011).
 - ¹³ P. Giannozzi, S. Baroni, N. Bonini, M. Calandra, R. Car, C. Cavazzoni, D. Ceresoli, G. L. Chiarotti, M. Cococcioni, I. Dabo, et al., *J. Phys.: Condens. Matter* **21**, 395502 (2009).
 - ¹⁴ R. D. Shannon, *Acta. Cryst.* **A32**, 751 (1976).
 - ¹⁵ A. M. Rappe, K. M. Rabe, E. Kaxiras, and J. D. Joannopoulos, *Phys. Rev. B Rapid Comm.* **41**, 1227 (1990).
 - ¹⁶ N. J. Ramer and A. M. Rappe, *Phys. Rev. B* **59**, 12471 (1999).
 - ¹⁷ <http://opium.sourceforge.net>.
 - ¹⁸ J. Ihm, A. Zunger, and M. L. Cohen, *J. Phys. C* **12**, 4409 (1979).
 - ¹⁹ J. P. Perdew and A. Zunger, *Phys. Rev. B* **23**, 5048 (1981).
 - ²⁰ H. J. Monkhorst and J. D. Pack, *Phys. Rev. B* **13**, 5188 (1976).
 - ²¹ P.-O. Löwdin, *J. Chem. Phys.* **18**, 365 (1950).
 - ²² D. Sanchez-Portal, E. Artacho, and J. M. Soler, *Solid State Communications* **95**, 685 (1995).
 - ²³ J. P. Perdew, K. Burke, and M. Ernzerhof, *Phys. Rev. Lett.* **77**, 3865 (1996).
 - ²⁴ P. K. Davies, *Curr. Opin. Solid State Mater. Sci.* **4**, 467 (1999).
 - ²⁵ I. Grinberg, M. R. Suchomel, P. K. Davies, and A. M. Rappe, *J. Appl. Phys.* **98**, 094111 (2005).
 - ²⁶ I. Grinberg and A. M. Rappe, *Phys. Rev. B* **70**, 220101 (2004), ISSN 0163-1829, URL <http://dx.doi.org/10.1103/PhysRevB.70.220101>.
 - ²⁷ I. Grinberg and A. M. Rappe, *Phys. Rev. Lett.* **98**, 037603 (2007).
 - ²⁸ L. Goncalves-Ferreira, S. A. T. Redfem, E. Artacho, E. Salje, and W. T. Lee, *Phys. Rev. B* **81**, 024109 (2010).
 - ²⁹ D. J. Singh, *Phys. Rev. B* **52**, 12559 (1995).